Threshold photoemission magnetic circular dichroism of perpendicularly magnetized Ni films on Cu(001): Theory and experiment

M. Kronseder,[1] J. Minár,[2] J. Braun,[2] S. Günther,[1] G. Woltersdorf,[1] H. Ebert,[2] and C. H. Back[1]

[1]*Department of Physics, Universität Regensburg, D-93040 Regensburg, Germany*

[2]*Department Chemie, Physikalische Chemie, Ludwig-Maximilians Universität München, D-81377 München, Germany*

(Received 18 January 2011; published 14 February 2011)

Threshold photoemission magnetic circular dichroism of perpendicularly magnetized Ni films on Cu(001) was measured in total electron yield and used to observe the magnetic domain structure in a photoemission electron microscope. Spin-polarized relativistic Korringa-Kohn-Rostoker Green's function calculations including a dynamical mean-field theory approach within the one-step-photoemission model reproduce the measured asymmetry in the photocurrents for left and right circularly polarized light. In addition, a three-step photoemission model calculation based on the same *ab initio* calculation is used to quantitatively explain the MCD effect near the photoemission threshold.

DOI: 10.1103/PhysRevB.83.132404 PACS number(s): 75.70.Ak, 71.15.Mb, 73.20.At, 78.20.Ls

The combination of exchange interaction and spin-orbit coupling gives rise to magnetic circular dichroism (MCD) in ferromagnetic materials. In a typical experiment an incoming photon with circular polarization promotes an initial state electron into an empty final state with a transition probability given by the dipole matrix elements. Since the spin-orbit interaction in core shells is large (∼15–20 eV) spin-split transitions can easily be separated and the resulting x-ray magnetic circular dichroism in ferromagnetic 3*d* transition metals is typically large (∼30 %) and easy to interpret. In the valence shell the spin-orbit interaction is much weaker (∼100 meV) and therefore the magneto-optical Kerr effect (MOKE) for visible light is typically very small (∼0.01%). However, it is also known that due to the large exchange splitting, MCD and magnetic linear dichroism (MLD) effects can be large in valence band photoemission. This enhancement is due to the narrow angular distribution of the photoelectrons as well as the energy selection compared to a photon-in photon-out technique such as MOKE which integrates over the entire *k*-space and does not allow for energy selection. Thus for particular materials and crystallographic orientations MCD and MLD effects can also be large in total yield valence band photoemission if the photon energy is tuned close to the work function of the material. In this case essentially only electrons propagating normal to the sample surface are selected in photoemission. Recently this has been demonstrated by Nakagawa *et al.* for the case of perpendicularly magnetized Ni/Cu(001)[1,2] and by Hild *et al.* for Co/Pt(111).[3] Threshold photoemission MCD (TP-MCD) asymmetries as large as 12% have been reported. These large asymmetries and the fact that the observed TP-MCD effects do not rely on the angular distribution of the photoelectrons make MCD in threshold photoemission a good candidate for the magnetic version of photoemission electron microscopy (PEEM) as has been demonstrated in Ref. 2. However, in order to fully exploit the potential of TP-MCD for photoemission microscopy, a method with enormous potential for laboratory-based high-resolution magnetic microscopy, it is essential to understand the contrast mechanism in detail. In this Brief Report, we compare our TP-MCD measurements on perpendicularly magnetized Ni/Cu(001) thin films to *ab initio* calculations using a one-step photoemission model as well as a three-step model. Due to the excellent agreement between experiment and theory, predictions for other material systems can be made. Furthermore we demonstrate high-resolution magnetic imaging in a PEEM. In addition, we can explain the peculiar dependence of the MCD asymmetry on the polarization state of the incident photons allowing to predict the polarization state leading to maximum asymmetry.

The experiments are conducted on a Cu(001) single-crystal disk which was cleaned by cycles of Ar ion sputtering at ∼1 keV and annealed at ∼800 K. Ni thin films were deposited onto the Cu(001) crystal by means of UHV-electron-beam evaporation. The deposition rate was ∼0.3 ML/min and controlled by measuring the molecular flux and by RHEED-oscillations. A sharp 1 × 1 RHEED structure was observed from clean, annealed Cu(001) and Ni/Cu(001) surfaces. The face-centered tetragonal Ni(001) on Cu(001)[4] undergoes a spin-reorientation transition from in-plane to out-of-plane magnetization at ∼7 ML[1,5] which is due to a small lattice mismatch of 2.5%. After film deposition the samples were transferred *in situ* into the photoemission electron microscopy (PEEM) chamber. In the PEEM chamber polar magneto-optical Kerr effect (MOKE) and magnetic circular dichroism (MCD) in both total electron yield (TEY) and spatially resolved by means of PEEM are measured. A laser diode [405 nm (3.06 eV), 50 mW power focused to a 2 by 4 mm^2 spot on the sample] was used for both MOKE and TP-MCD measurements. MOKE and TP-MCD hysteresis loops for a 16ML Ni/Cu(001) sample, Fig. 1(a), show both square hysteresis loops with nearly identical coercive fields H_C ∼ 100 Oe. In order to extract photoelectrons the work function of the samples [for Ni(001) ∼4.95 eV[6]] has to be lowered. This was achieved by depositing a fraction of a ML of Cs onto the Ni film in the PEEM chamber. The lowest possible work function for cesiated Ni is ∼1.4 eV.[7] The effect of the dipolar field established by Cs adatoms to decrease the work function is very longlasting and stable for photon energies in the range of 3 eV. It was possible to perform TP-MCD measurements more than 3 weeks after first Cs deposition without a significant decrease of the obtained photocurrents and TP-MCD asymmetries. This is quite different for photon energies below ∼2.0 eV, where the threshold of photoemission and the TP-MCD-asymmetry peak is close to the minimum work function of cesiated Ni.[7]

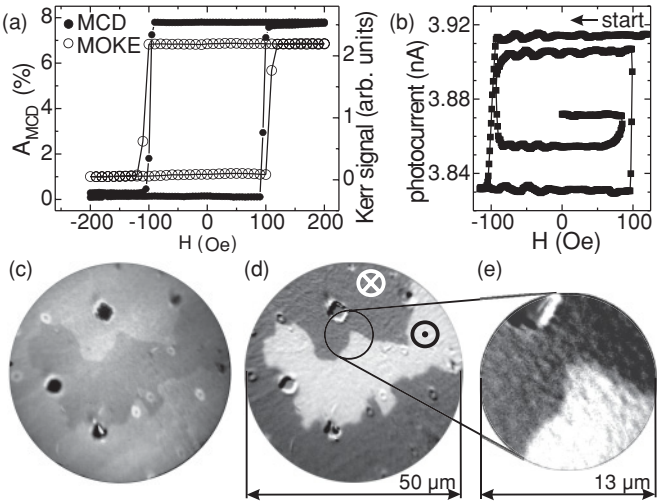

FIG. 1. (a) Hysteresis loops of 16ML Ni/Cu(001), taken with *rcp* light. The coercive fields of ∼100 Oe are nearly equal for both, MOKE (open circles) and TP-MCD-TEY (filled circles) measurements. The incidence angle of the laser light (405 nm) is 65° with respect to the sample surface normal. (b) Demagnetizing hysteresis loop of the same sample measured with TP-MCD-TEY. In the demagnetized state the magnetization within the laser spot is composed of magnetic domains. (c) PEEM image taken with *rcp* light (405 nm). (d) TP-MCD image. (e) Zoomed in image.

The MCD asymmetry is defined as[8]

$$A_{\mathrm{MCD}} = \frac{I(\uparrow\uparrow) - I(\uparrow\downarrow)}{I(\uparrow\uparrow) + I(\uparrow\downarrow)} = \frac{I(\downarrow\downarrow) - I(\downarrow\uparrow)}{I(\downarrow\downarrow) + I(\downarrow\uparrow)}, \qquad (1)$$

where $I(\mathbf{M},\mathbf{h})$ are the photocurrents obtained by parallel (antiparallel) alignment of the magnetization direction and the photon spin [$I(\uparrow\uparrow)$ and $I(\uparrow\downarrow)$, respectively]. The latter equation leads to $A_{\mathrm{MCD}} \sim \mathbf{M}\cdot\mathbf{h}$, where $\mathbf{h}$ is the helicity of the incoming photons and $\mathbf{M}$ is the magnetization direction. Magnetization $\uparrow(\downarrow)$ means a magnetization direction out-of-plane (into-the-plane) and helicity $\uparrow(\downarrow)$ corresponds to right (left) circularly polarized [*rcp* (*lcp*)] light. The image in Fig. 1(c) is obtained with PEEM by illuminating the sample with *rcp* light. This demonstrates that even in real time view, i.e., without subtracting images or using Eq. (1), a magnetic contrast is visible. By applying Eq. (1) to two images taken with *rcp* and *lcp* light, respectively, one obtains image Fig. 1(d) and 1(e). In the latter the PEEM is set to approximately four times higher magnification.

The fact that the asymmetry depends on the helicity projected onto the magnetization in combination with an incidence angle of 65° with respect to the surface normal given by the geometry of the PEEM instrument leads to a peculiar dependence of the asymmetry on the incoming polarization state, as shown in Fig. 2(c). The origin of this behavior is that the asymmetry depends only on the photon polarization state *inside* the material which is generally different from the incident polarization state. By using Fresnel's formulas and Snell's law for absorptive media (complex refractive index), we determine the degree of circularity of the transmitted photons for various incident polarization states.[9] In the computation the perpendicular ($A_\perp$) and the parallel ($A_\parallel$) part of the incident wave are separated with respect to the incidence plane, see

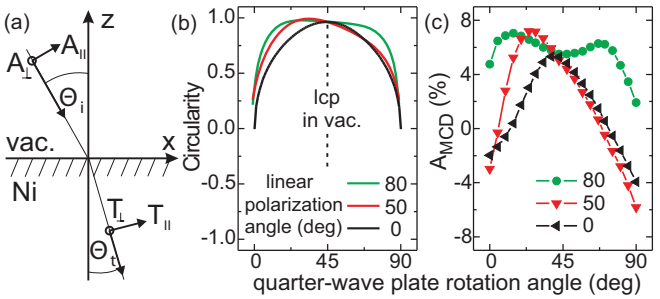

FIG. 2. (Color online) (a) Coordinate system used for the calculation. The incident polarization state, fully described by $A_\perp$ and $A_\parallel$, can be set in the experiment by a rotatable linear polarizer and a rotatable quarter-wave plate. (b) Theoretical dependence of the circularity on the incident polarization state, when the incidence angle $\theta_i = 65°$. (b) Experimental dependence of the MCD-asymmetry A_{MCD} on the incoming photon polarization state. Both, (b) and (c), shown for different angles of the linear polarizer (80°, 50°, 0°) with respect to the incident plane, in (a) the z-x plane.

Fig. 2(a). In doing so, the transmitted parts ($T_\perp$ and $T_\parallel$) acquire additional phases. A second projection onto the magnetization axis (for out-of-plane magnetized samples) must be included as well. The refractive index for Ni and 3.06 eV is $n(1 - i\kappa) = 1.61(1 - i2.39)$.[10] In the experiment the incident polarization state is set by a linear polarizer and a quarter-wave plate. The results of the calculated degree of circularity and the experimentally determined MCD asymmetry are plotted in Fig. 2(b) and 2(c) for three individual linear polarization angles for a rotation angle range from 0 to $\frac{\pi}{2}$ of the quarter-wave plate with respect to the linear polarizer. Despite the fact that we calculated only the degree of circularity with respect to the transmission angle, according to Ref. 11, the results of experiment and theory are in qualitative agreement with respect to the peaks appearing in the graphs (e.g., the unexpected double peak structure for an incident angle of 80°). We note at this point that the photoemission process itself is not included in these calculations, yet.

The underlying physical mechanism of TP-MCD is of general interest since it concerns many applications. It does not only enable a PEEM to investigate magnetic samples in a very compact setup, TP-MCD is also exploited in time-resolved photoemission measurements in low energy electron spectroscopy as well as in ultrafast-MOKE measurements.[12] Therefore, to shed light on the underlying microscopic processes we demonstrate in the following the capability of *ab initio* theory to explain MCD in threshold photoemission. Calculations are performed within two individual photoemission models, at first in a one-step model and then in a three-step model. The one-step model accounts for all effects of the photoemission process as for example dipole selection rules and surface emission.[13] The electronic structure results from a spin-polarized relativistic Korringa-Kohn-Rostoker Green's function (SPR-KKR) method[14] and was calculated self-consistently within the local spin-density approximation in combination with the dynamical mean-field theory (LSDA + DMFT).[15–17] The theoretical key results are shown in Fig. 3(c)–3(g) and compared to measurements (a) and (b). In the calculations a photon energy of 3.06 eV (405 nm)

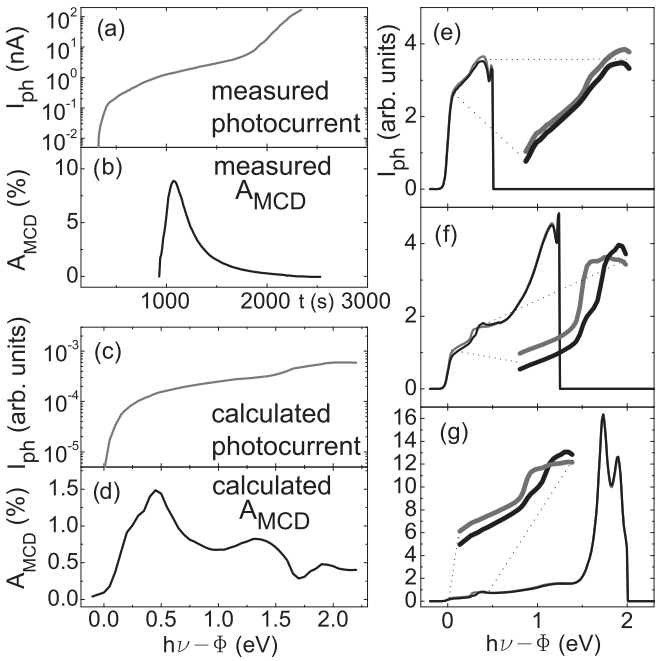

FIG. 3. (a) and (b) The photocurrent and TP-MCD asymmetry obtained as a function of Cs-deposition time. Before ∼900 s the signal-to-noise ratio with an applied magnetic field was to low. The one-step model calculations of dichroic signal and yield are shown in (c) and (d), respectively. In (e)–(g) the spherically averaged spectra for right (red) and left (black) circularly polarized light for work function values Φ of 2.5 eV (e), 1.75 eV (f), and 1.0 eV (g) are shown.

is used. Since in the present experiment we are not able to measure the photoemission spectra as a function of energy, we plot the experimental data as a function of Cs deposition time. However, by comparing the photoemission threshold in (a) and (c) and also the peaks of the TP-MCD asymmetry curves shown in (b) and (d) we conclude that the experimental TP-MCD asymmetry has its maximum at 0.4–0.5 eV. At this point we would like to note that the experimental TP-MCD curve Fig. 3(b) was measured by reversing the magnetization instead of changing the helicity of the incident photons, which was set to *right* circular polarization.

Each point in the theoretically calculated photocurrent shown in Fig. 3(c) represents an integral over the allowed range of binding energies spherically averaged to simulate the total experimental yield. To illustrate this procedure we present in Fig. 3(e)–3(g) spherically averaged spectra for *right* (red) and *left* (black) circularly polarized light for work function values Φ of 2.5 eV (e), 1.75 eV (f), and 1.0 eV (g). All spectra start with a plateau-like region and reveal the maximum dichroic signal around 0.5 eV binding energy, shown as inset. The dominant spectral feature visible in each case close to the highest binding energy is mainly due to a *d*-like surface resonance[15,18] which shifts as a function of Φ and strongly increases in intensity for greater Φ values. From this the kink-like increase in the yield at about 1.5 eV becomes explainable because each point in the total yield plot represents the accumulated intensity distribution from a complete spectrum as shown in panels (e)–(g). The moderate increase in the calculated yield appears more pronounced in the experiment most probably since theory underestimates the intensity variation of the surface resonance with Φ. With the same argument the deviation in the maximum value of the dichroic signal can be understood. Concerning the energetics the agreement is quantitative, reflecting therewith the accurate description of electronic correlations in Ni through the LSDA + DMFT method.[15]

The one-step photoemission model reproduces the energy dependence of photocurrent and TP-MCD asymmetry. However, this model does not allow for a simple physical explanation for the MCD-effect near the Fermi level. Therefore a simpler three-step model of photoemission is used to further investigate the physical origin of TP-MCD. In this model the photoemission process is separated into transmission and absorption of light and the emission of the excited electrons. Since the major contribution to the MCD asymmetry originates in the absorption process, we investigate in this simple model only the available initial states involved in the photoemission process. The spin polarization of the initial states is a measure of the TP-MCD asymmetry for the following reason: the photon helicity couples to the spin of the electrons via spin-orbit coupling and the spin polarization itself results from the magnetization. Therefore the larger the spin polarization, the larger the TP-MCD asymmetry. The spin polarization can be calculated by subtracting surface-projected Bloch-spectral functions for spin-up and spin-down states. The Bloch-spectral function can be viewed as the

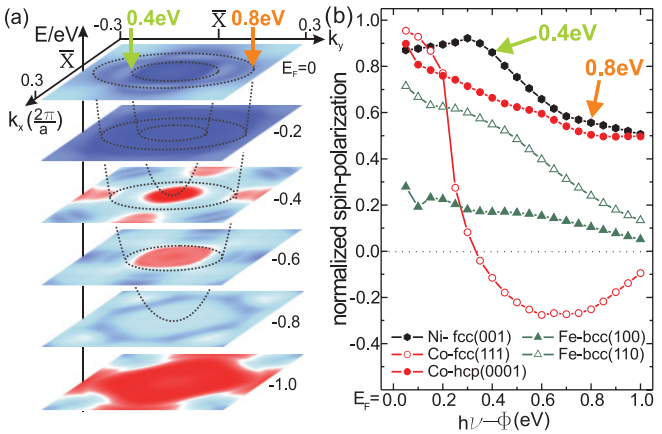

FIG. 4. (Color) (a) The LSDA + DMFT spin polarization (minority minus majority electrons) of the surface-projected Bloch spectral function of out-of-plane magnetized *fcc*-Ni(001) is shown for different energies below the Fermi level E_F. Blue color means more minority electrons, and red color means more majority electrons. Due to the energy-wave-vector relation in the free-electron approximation $E = \frac{\hbar^2 k_i^2}{2m}$, the available initial k_i vectors of the photoemission process are within a paraboloid, schematically shown in (a) for 0.4 eV (green) and 0.8 eV (orange). The dependence of the normalized spin polarization within those paraboloids on the maximum kinetic energy of the photoelectrons are plotted in (b) for *fcc*(001)-Ni, *fcc*(111)- and *hcp*(0001)-Co as well as for *bcc*(100)- and *bcc*(110)-Fe, where $h\nu$ is the photon energy and Φ is the work function. All calculations are done with LSDA + DMFT and for out-of-plane magnetization. The arrows in (b) indicate the calculated spin-polarization values for the paraboloids shown in (a).

k-dependent density of states (DOS) function. In Fig. 4(a) subtracted LSDA+DMFT Bloch spectral functions, i.e., the spin polarization, for *fcc*-Ni are plotted for various energies below the Fermi energy E_F. The main result from the plot in Fig. 4(a) is the reversal of the spin polarization between 0.2–0.4 eV in some **k** regions. By lowering the work function with the aid of Cs, one increases the energetic range of low-energy photoelectrons and therefore more states below E_F are accessible. Since in the photoemission process the initial-state vector k_i is coupled to the final-state vector k_f by an energy and wave-vector conserving transition, the available initial k_i vectors are located within a paraboloid, described by the energy-wave-vector relation in the free-electron approximation $E = \frac{\hbar^2 k_\perp^2}{2m}$, where $k_\perp = \sqrt{k_x^2 + k_y^2}$ is the magnitude of the electron-wave vector perpendicular to the surface and m is the electron mass. For a specified penetration depth the spin polarization of the initial states results from the summation of all spin-polarization values within the paraboloids normalized to all available states within the corresponding paraboloid. Figure 4(b) summarizes these summations for different work functions at a fixed photon energy. This plot reveals that the maximum TP-MCD asymmetry should be achieved at ∼0.3–0.4 eV. By way of comparison the agreement between both photoemission models, Figs. 3(d) and 4(b), are very good. In addition, the three-step photoemission model calculation allows also for a simple explanation of the TP-MCD effect near the Fermi level, i.e., the spin polarization in this energy region. Due to this qualitative agreement, we are able to predict the MCD contrast of various other materials as shown in Fig. 4(b) for *fcc*(111)- and *hcp*(0001)-Co or *bcc*(100)- and *bcc*(110)-Fe. Co-*fcc*(111) exhibits an opposite spin polarization with respect to all other materials below 0.3 eV. In fact, the opposite sign of the asymmetry has already been verified experimentally in one particular experimental setup, compare Ref. 1 for Ni and Ref. 3 for Co-*fcc*(111). However, the reversal around 0.3–0.4 eV for the latter has not been observed, which might be attributed to experimental difficulties in determining the work function. Note that we carefully examined the circularity and magnetization direction in order to determine the sign resulting from Eq. (1).

Concluding we have shown that TP-MCD can be used for efficient table top high resolution magnetic microscopy using PEEM. *Ab initio* calculations allow us not only to explain the observed TP-MCD asymmetries, but also to predict asymmetry values for various materials. The large measured and predicted TP-MCD asymmetries may allow high-resolution time-resolved imaging in these material systems. Clearly more experimental work has to be performed to demonstrate the power of this new experimental method for fast high-contrast magnetic imaging. In particular it has to be demonstrated that covering the magnetic films with minute amounts of Cs does not change the magnetic domain configuration.

Financial support by the Deutsche Forschungsgemeinschaft through FOR 1346 and MI-1327/1 is gratefully acknowledged.

[1] T. Nakagawa and T. Yokoyama, Phys. Rev. Lett. **96**, 237402 (2006).
[2] T. Nakagawa, T. Yokoyama, M. Hosaka, and M. Katoh, Rev. Sci. Instrum. **78**, 023907 (2007).
[3] K. Hild *et al.*, Phys. Rev. B **82**, 195430 (2010).
[4] M. Farle, W. Platow, A. N. Anisimov, P. Poulopoulos, and K. Baberschke, Phys. Rev. B **56**, 5100 (1997).
[5] F. Huang, M. T. Kief, G. J. Mankey, and R. F. Willis, Phys. Rev. B **49**, 3962 (1994).
[6] C. A. Papageorgopoulos and J. M. Chen, Solid State Commun. **13**, 1455 (1973).
[7] L. W. Swanson and R. W. Strayer, J. Chem. Phys. **48**, 2421 (1968).
[8] W. Kuch *et al.*, Phys. Rev. B **53**, 11621 (1996).
[9] M. Born and E. Wolf, *Principles of Optics* (Pergamon Press, Oxford, 1980).
[10] E. D. Palik, *Handbook of Optical Constants of Solids* (Elsevier, Amsterdam, 1998).
[11] D. T. Pierce *et al.*, Rev. Sci. Instrum. **51**, 481 (1980).
[12] U. Bovensiepen, J. Phys. Condens. Matter **19**, 083201 (2007).
[13] J. F. L. Hopkinson, J. B. Pendry, and D. J. Titterington, Comput. Phys. Commun. **19**, 69 (1980).
[14] The Munich SPR-KKR package, version 5.4, H. Ebert *et al.* [http://ebert.cup.uni-muenchen.de/ak/ebert/SPRKKR].
[15] J. Braun, J. Minár, H. Ebert, M. I. Katsnelson, and A. I. Lichtenstein, Phys. Rev. Lett. **97**, 227601 (2006).
[16] M. Pickel *et al.*, Phys. Rev. Lett. **101**, 066402 (2008).
[17] J. Sánchez-Barriga *et al.*, Phys. Rev. Lett. **103**, 267203 (2009).
[18] E. W. Plummer and W. Eberhardt, Phys. Rev. B **20**, 1444 (1979).